HHS Public Access

Author manuscript

Gut. Author manuscript; available in PMC 2020 October 01.

Published in final edited form as:

Gut. 2020 October ; 69(10): 1750–1761. doi:10.1136/gutjnl-2019-318817.

MiR130b from Schlafen4+ MDSCs stimulates epithelial proliferation and pre-neoplastic changes before gastric cancer

Lin Ding[*,1,3], **Qian Li**[*,2], **Jayati Chakrabarti**[4], **Andres Munoz**[3], **Emmanuelle Faure-Kumar**[5], **Ramon Ocadiz-Ruiz**[1], **Nataliya Razumilava**[1], **Guiying Zhang**[2], **Michael M. Hayes**[1], **Erica A Sontz**[3], **Zoe Elena Mendoza**[3], **Swapna Mahurkar-Joshi**[5], **Joel K Greenson**[6], **Guillermo I. Perez-Perez**[7], **Nguyen Thi Hong Hanh**[8], **Yana Zavros**[4], **Linda C. Samuelson**[9], **Dimitrios Iliopoulos**[5,10], **Juanita L. Merchant**[1,3,9]

[1:]Dept of Internal Medicine-Gastroenterology University of Michigan, Ann Arbor

[2:]Xiangya Hospital, Central South University, China

[3:]Dept of Medicine-Gastroenterology, University of Arizona, Tucson

[4:]Dept of Pharmacology and Systems Physiology, University of Cincinnati, Cincinnati

[5:]Dept of Medicine-Digestive Diseases, UCLA

[6:]Dept of Pathology, University of Michigan, Ann Arbor

[7:]New York University School of Medicine, NYU School of Medicine, NY

[8:]Dinh Tien Hoang Institute of Medicine, Vietnam Union of Science and Technology Association; Institute of Biotechnology, VietNam Academy of Science and Technology

[9:]Dept of Molecular and Integrative Physiology, University of Michigan, Ann Arbor

[10:]Kynan Pharmaceuticals, Northridge, CA

Abstract

Summary: The myeloid differentiation factor Schlafen4 (Slfn4) marks a subset of Myeloid Derived Suppressor Cells (MDSCs) in the stomach during *Helicobacter*-induced spasmolytic polypeptide-expressing metaplasia (SPEM).

Objective: To identify the gene products expressed by Slfn4+-MDSCs and to determine how they promote SPEM.

Design: We performed transcriptome analyses for both coding genes (mRNA by RNA-Seq) and non-coding genes (microRNAs using NanoString nCounter) using flow-sorted SLFN4^{+} and

Corresponding Author: Juanita L. Merchant, MD, PhD, 1501 N. Campbell Ave, P.O. Box 245028, Tucson, AZ 85724-5028, jmerchant@email.arizona.edu, Ph. 520-626-3334, F 520-626-1291.

*Contribute equally to the work

Author Contributions

LD and QL designed research studies, conducted experiments, analyzed data, and wrote the manuscript. AM, YZ, JC and ZM performed xenograft-related experiments. EFK, SMJ, NR and DI performed microRNA analysis. ROR conducted organoid experiments. MH and ES performed mouse breeding and genotyping. JKG read the histology. GIPP ran the Hp IgG analysis. GZ, NTHH and LS collected and provided clinical samples. JLM designed research studies and wrote the manuscript.

Declaration of Interests

The authors have declared that no competing interests exist.

SLFN4^{-} cells from *Helicobacter*-infected mice exhibiting metaplasia at 6 months post-infection. Thioglycollate-elicited myeloid cells from the peritoneum were cultured and treated with IFNα to induce the T cell suppressor phenotype, expression of MIR130b and SLFN4 were evaluated. MIR130b expression in gastric tissues and human patient sera was determined by qPCR and *in situ* hybridization. In vivo knockdown of MiR130b in *Helicobacter*-infected mice was performed via Invivofectamine. Organoids from primary gastric cancers were used to generate xenografts. ChIP assay and Western blots were performed to demonstrate the activation of NFκb p65 by MIR130b.

Results: MicroRNA analysis identified an increase in MiR130b in gastric SLFN4^{+} cells. Moreover, MIR130b co-localized with SLFN12L, a human homolog of SLFN4, in gastric cancers. MiR130b was required for the T-cell suppressive phenotype of the SLFN4^{+} cells and promoted *Helicobacter*-induced metaplasia. Treating gastric organoids with the MIR130b mimic induced epithelial cell proliferation and promoted xenograft tumor growth.

Conclusion: Taken together, MiR130b produced by SLFN^{+}-myeloid cells plays an essential role in MDSC function and supports metaplastic transformation prior to gastric cancer.

Keywords

microRNA130b; Schlafen; MDSCs; gastric cancer

Introduction:

Metaplastic changes in the stomach typically follow chronic inflammation initiated by *Helicobacter* and precedes neoplastic transformation. We previously reported that a subset of Hedgehog(Hh)-Gli1-dependent immune cells are recruited to the gastric epithelium during *Helicobacter* infection in mice and polarize into myeloid-derived suppressor cells (MDSCs)[1], an event that coincides with parietal cell atrophy and spasmolytic polypeptide-expressing metaplasia (SPEM)[2]. MDSCs are a heterogeneous population of immature myeloid cells[3], and a subset increase their expression of Schlafen4 (SLFN4). SLFNs are a family of molecules strongly induced by type 1 interferons (IFNα), which has been implicated in lymphoid and myeloid cell development and differentiation[4]. In particular, SLFN4 is a myeloid cell differentiation factor that regulates myelopoiesis[5]. We previously demonstrated that SLFN4^{+} cells originate in the bone marrow, migrate to the stomach during *Helicobacter* infection and require Hh signaling. By sorting fluorescently-tagged SLFN4^{+} cells from the stomachs of *Helicobacter*-infected mice,, we showed that recruited SLFN4^{+} cells acquire their T cell suppressor phenotype by 4-6 months following infection[6]. Similar to murine SLFN4, protein expression of the human homolog SLFN12L increases in *H. pylori*–infected patients with intestinal metaplasia and also marks a population of MDSCs[6].

Ostensibly, the immune suppressive function of MDSCs emerges to dampen the active inflammatory process upon presumed resolution of the *Helicobacter* infection. However, inherent in resolving the mucosal damage, secretion of pro-proliferative signals from the myeloid cells creates a permissive environment for hyperplasia, metaplasia and eventually tumor formation[7]. To define the underlying mechanism that drives the emergence of this myeloid cell sub-population and investigate its role in tumor progression, we performed

transcriptome analyses for both coding genes (mRNA by RNA-Seq) and non-coding genes (microRNAs using NanoString nCounter) using flow-sorted SLFN4^{+} and SLFN4^{-} myeloid cells from the stomachs, bone marrow and spleens of *Helicobacter*-infected mice. MicroRNAs (miRNAs) are endogenous small, noncoding RNAs that negatively regulate target gene expression. Secreted miRNAs are recognized as mediators of intercellular communication[8]. Given their stability in the blood, they can serve as stable circulating biomarkers of disease[9]. Here we show that SLFN4^{+}-MDSCs isolated from the metaplastic mouse stomach express MiR130b. Moreover, we identified elevated levels of MIR130b in the serum of both *Helicobacter*-infected mice and human patients that correlated with the respective metaplastic changes in the stomach. MIR130b is required for MDSC-mediated function and the metaplastic changes prior to gastric cancer.

Results:

RNA profiling of SLFN4^{+} and SLFN4^{-} cells

We flow-sorted SLFN4-tdTomato^{+} (SLFN4^{+}) and SLFN4-tdTomato^{-} (SLFN4^{-}) myeloid cells (CD11b^{+}) from the stomachs, bone marrow and spleens of *Slfn4-CreERT2:Rosa-LSL-tdTomato* mice infected with *Helicobacter felis* (*H. felis*) for 6 months. The cells were profiled using two high throughput genome-wide analyses (RNAseq and miRNA Nanostring nCounter).

RNAseq identified over 5000 differentially-expressed genes (fold change >2) from stomach SLFN4^{+} (ST4+) compared to bone marrow SLFN4^{+} (BM4+) and splenic SLFN4^{+} cells (SP4+) as well as stomach SLFN4^{-} cells (ST4−) (Fig.S1A). The hierarchical clustering heat map displayed distinct transcriptome profiles for ST4+ cells (Fig.S1B), suggesting that a distinct gene expression signature was acquired in the stomach. Many of the highly induced transcripts identified in the ST4+ cells were consistent with MDSC polarization (Fig. S1C). A subset of these genes was validated by qPCR (Fig. S1D–L). Of note MDSCs express high levels of inducible nitric oxide synthase (NOS2) and arginase I (ARG1), which consume L-arginine in the microenvironment to produce nitric oxide and reactive oxygen species (ROS)[10]. Reduced L-arginine blocks TCR-ζ chain synthesis and T cell proliferation. Transcripts encoding these two major effector enzymes, especially NOS2, were highly expressed in the gastric ST4+ myeloid cells, but were significantly less in the bone marrow and spleen, consistent with our prior findings that acquisition of MDSC function occurs in the stomach[6].

Using the Nanostring nCounter profiling, we found that differences in microRNA expression in ST4+ cells differed from the BM4+ and SP4+ gene signatures (Fig.1A). Thirty-five differentially-expressed miRNAs (>2-fold) were identified by comparing ST4+ cells to ST4− cells. Moreover, 36 transcripts were differentially-expressed by comparing ST4+ to the BM4+ and SP4+ cells (Fig. 1B). Of the 13 miRNAs that overlapped between the two groups, 12 miRNAs were significantly down-regulated while only *Mir130b* was exclusively upregulated (Fig.1B).

MiR130b correlates with mouse SLFN4 and human SLFN12L expression

To determine whether *MiR130b* expressed in the gastric SLFN4$^+$-MDSCs correlated with its expression in serum, MiR130b expression was measured in gastric extracts and serum across 6 months following *H. felis* infection. MiR130b increased in both the sera and gastric tissues from infected mice (Fig.S2), which occurred coincided with *Slfn4* mRNA induction and to the appearance of *Helicobacter*-induced SPEM as previously reported[6]. Thioglycollate-elicited (TG) peritoneal cells were treated ex vivo with IFNα to induce myeloid cell polarization[6], and demonstrated that peak expression for both *Slfn4* and MiR130b occurred within 24h (Fig.2A). MiR130b *in situ* hybridization was performed and MiR130b was shown to localize to the SLFN4$^+$ myeloid cells (Fig.2B). To determine if these SLFN4$^+$ MDSCs released MiR130b, SLFN4$^+$ and SLFN4$^-$ cells were flow-sorted after treating the naïve TG peritoneal myeloid cells with IFNα for 24 hours. The amount of MiR130b found in the media of the SLFN4+ cells was 4.5-fold higher than the amount present in the SLFN4$^-$ media (Fig.2C). Since *Slfn4* is a Gli1-dependent gene inducibly regulated by IFNα[16], we showed that MiR130b expression in SLFN4$^+$ cells was also Gli1-dependent by treating the peritoneal myeloid cells isolated from *Gli1*$^{-/-}$*:Slfn4*-tdTomato$^+$ versus *Slfn4*-tdTomato$^+$ mice with IFNα (Fig.S3A).

MIR130b was also highly expressed in gastric cancer compared to normal tissue (Fig.2D). Since *SLFN12L* is the closest human homolog of mouse *Slfn4* and also marks human MDSCs[6], we co-localized SLFN12L protein with MIR130b by *in situ* hybridization in the stroma surrounding gastric cancer cells (Fig.2E). MIR130b and SLFN12L were also co-expressed in the HL-60 human myeloid line after co-culturing with *H. pylori* (Fig.S3B). Knockdown of *GLI1* prevented *SLFN12L* and MIR130b mRNA expression in the presence of *H. pylori* (Fig.S3B, C). Moreover, similar to *Slfn4*, IFNα strongly induced *SLFN12L* (Fig.S3D, E). HL-60 cells treated with *H. pylori* with or without the *GLI1* inhibitor GANT61 or *GLI1* siRNA blocked both MIR130b and *SLFN12L* induction, indicating that MIR130b expression correlates with *Slfn4* and *SLFN12L* expression in a *GLI1*-dependent manner.

We used qPCR to determine the levels of *MIR130b* in archived sera collected from 115 Vietnamese patients with gastritis, atrophy or atrophy plus intestinal metaplasia (Table S1 and Fig.2F) and found significantly elevated serum levels of MIR130b only in patients with atrophy and metaplasia. Furthermore, analysis of a cohort of Chinese gastric cancer patients similarly demonstrated elevated serum levels of MIR130b (Table S2 and Fig.2G). Therefore, as observed in *Helicobacter*-induced SPEM in mice, elevated MIR130b levels were observed in the serum of patients with intestinal metaplasia and cancer.

MIR130b is essential for SLFN$^+$-MDSC activity

As previously reported, *Slfn4* is highly induced in peritoneal myeloid cells treated with IFNα and acquire the ability to suppress T cell proliferation[6]. Therefore to examine the functional effect of the microRNA on SLFN4$^+$ cells, we compared the effect of knocking down endogenous MiR130b during IFNα induction of Slfn4 to MiR130b overexpression with the mimic. Knocking down *Slfn4* with siRNA abolished the induction of MiR130b, however knocking down MiR130b did not inhibit *Slfn4* induction by IFNα, indicating that

Slfn4 was required for MiR130b induction (Fig.3A). IFNα, but not treatment with the MiR130b mimic induced *Arg1* and *Nos2* expression. However, both *Slfn4* or MiR130b antisense abolished the IFNα induction of these two mRNAs, demonstrating a requirement for MiR130b and *Slfn4* in the expression of enzyme characteristic of MDSCs function. To determine directly whether SLFN4$^+$-MDSCs require MiR130b for T cell suppressor function, we flow-sorted SLFN4$^+$ and SLFN4$^-$ cells from TG peritoneal myeloid cells treated with IFNα and co-cultured them with T cells after transfecting with MiR130b mimic, antisense or scrambled oligos (Fig.3B). As expected, Tregs (splenic CD4$^+$CD25$^+$) inhibited T cell proliferation (Fig.3C,D). Flow-sorted SLFN4$^+$ cells inhibited T cell proliferation by 60% (from 57.4% to 22%), however, no significant T cell suppression was observed when SLFN4$^-$ cells or untreated TG peritoneal myeloid cells were co-cultured with activated T cells (Fig.3, NT). Transfecting SLFN4$^-$ cells with the MiR130b mimic was not sufficient to impart the T cell suppressor phenotype to these cells. However, SLFN4$^+$ cells transfected with the MiR130b antisense oligo exhibited only minimal T cell suppression. Therefore, MiR130b was required but not sufficient for the SLFN4$^+$ cells to exhibit the MDSC T cell suppressor phenotype. To further test the effect of MiR130b, we knocked down MiR130b *in vivo* by IP injecting mice infected with *Helicobacter* for 4 months with antisense MiR130b using Invivofectamine reagent. Knockdown of MiR130b in the stomach was validated by qPCR at 3 weeks after transfection (Fig.S4). Suppression of MiR130b was sufficient to restore CD8$^+$ cytotoxic T cell infiltration of the stomach (Fig.3E), suggesting impaired MDSC function. Less SPEM developed after knocking down MiR130b *in vivo* as demonstrated by reduced Clusterin and co-expression of CD44 with GSII at the base of gastric glands (Fig.3F) as well as less *Tff2*, Clusterin (*Clu*) and CD44v9 mRNA expression without significant recovery of parietal and chief cell markers H/K-ATPase α subunit (*Atp4a*), *Gif*, respectively (Fig.S5).

MIR130b promotes gastric epithelial cell proliferation and xenograft tumor formation

Since MIR130b was detected in the media of cultured SLFN$^+$-MDSCs, we tested whether MIR130b exerts a proliferative effect on gastric epithelial cells in addition to regulating MDSC activity. Gastric cell proliferation was measured after transfecting AGS cells, a human gastric cancer cell line, and non-transformed mouse or human gastric organoids with MIR130b mimic or antisense. The MIR130b mimic induced AGS cell proliferation, while addition of MIR130b antisense decreased proliferation (Fig.S6). Proliferating cells within gastric organoids from normal mice or human subjects were labelled with EdU and quantified by immunofluorecent staining and flow cytometry. MIR130b mimic doubled the number of proliferating cells, while the antisense did not significantly affect proliferation (Fig.4A, Fig.S7). Mouse gastric organoids were then co-cultured with flow-sorted SLFN4$^+$ or SLFN4$^-$ cells prepared after treating the TG peritoneal myeloid cells from the *Slfn4-tdTomato* mice with IFNα in transwell cultures. The 0.4μm pore size of the insert membrane permitted diffusion of soluble factors from myeloid cells in the upper chamber to the lower chamber containing mouse organoids, while preventing the transfer of any cells. After 48h, mouse gastric organoids co-cultured with IFNα-induced SLFN4$^+$ cells exhibited a greater number of proliferating cells than organoids cultured with SLFN4$^-$ cells (Fig.4B). Knocking down MIR130b significantly reduced this induction. Thus SLFN4$^+$-MDSCs secreted *MiR130b*, which was capable of promoting gastric epithelial proliferation.

Next, we examined the effect of MIR130b using a xenograft tumor model generated with patient-derived organoids from human gastric cancers (diffuse, intestinal, signet ring). Organoids were pretreated with either scrambled, MiR130b mimic or antisense oligos before injecting into the right flank of immune-deficient NSG mice. Xenograft tumor volumes from 3 different organoid lines are shown in Fig.4D–F. Tumor growth was observed in the scrambled group. However, the mimic-treated group doubled their tumor size while few antisense-treated organoids developed into tumors (Fig.4C,D). To rule out the possibility that organoids in the antisense group were not viable, a cell viability assay was performed on organoids transfected with mimic, antisense, or scrambled sequences prior to xenograft transplantation. All groups exhibited 60%-70% viability after transfection (Fig.S8). Immunofluorescence using an antibody specific for human histone H3 confirmed engraftment of human-derived cells (Fig.S9). Although differences in the MIR130b serum levels were not statistically significantly, the microRNA levels in xenograft tumors were significantly higher in the mimic group and knocked down in the antisense group. (Fig.4G). Collectively, MIR130b exhibited a pro-proliferative effect on gastric epithelial cells; while reducing MIR130b tissue levels exerted a remarkable anti-tumor effect.

MIR130b targets Cylindromatosis (Cyld) and induces NFκb activity

TargetScan v7.0 was used to predict direct downstream gene targets that MIR130b potentially regulates. A heatmap was generated showing MIR130b gene targets from the public database that overlapped with transcripts differentially expressed in our RNA-seq data (Fig.5A). The tumor suppressor genes *Runx3, Trp53inp1, Cebpε, Pten* and *Cyld* are previously reported *MIR130b* targets in various tissues [11–17], and were expressed in the ST4+ cells at much lower levels than the BM4+ and SP4+ cells. Transfecting SLFN4^{+} peritoneal myeloid cells with the MIR130b mimic or antisense oligos showed that the mimic significantly suppressed *Cyld* and *Trp53inp1*, suggesting that they might be the relevant direct targets of MIR130b in these myeloid cells (Fig.S10). Indeed, the *cylindromatosis* gene (*CYLD*) encodes a deubiquitinating enzyme that inhibits ubiquitination of Iκb and retains the NFκb heterodimer p65/p50 in the cytoplasm (Fig.5B). *Cyld* was recently shown to be a bona fide target of *MIR130b* and that the NFκb subunit p65 was a potential regulator of the *MIR130b* locus[1318]. Therefore, we determined whether there is a feedback loop between NFκb activation and *MIR130b* expression, by using the human myeloid HL-60 cell line. The three predicted NFκb binding sites (BS) in the MIR130b promoter region are shown[13] (Fig.5B). To determine whether NFκb bound to these promoter sites, HL-60 cells were transfected with scrambled or MIR130b mimic prior to performing chromatin immunoprecipitation (ChIP). The Iκb promoter was used as a positive control for NFκb binding while GAPDH was used as a negative control. NFκb physically bound to the *MIR130b* promoter, and the binding activity was enhanced by overexpressing MIR130b (Fig.5C). Interestingly, the *NOS2* promoter is also a NFκb target[19]. Accordingly, MIR130b overexpression also induced binding of NFκb to both the *Nos2* and *Iκb* promoters, suggesting that MIR130b increases the DNA binding activity of NFκb (Fig.5C). The MIR130b mimic also induced NFκb p65 expression, while knocking down endogenous MIR130b reduced basal levels of p65 and blocked induction by TNFα (Fig.5D). These results demonstrated that NFκb induces *MIR130b* expression by directly binding to its promoter, and that MIR130b subsequently induces NFκb expression and activity.

Western blotting of cytoplasmic and nuclear extracts from xenograft tumors showed that NFκb translocates to the nucleus in the mimic-treated group (Fig.5E,F). We observed higher expression of NFκb in both the cytoplasm and nucleus, which inversely correlated with CYLD expression, suggesting that increased NFκb activity contributed to accelerated tumor growth observed with the MIR130b mimic.

Discussion

SLFN4 is a known myeloid differentiation factor and T cell quiescence factor[146]. We previously reported that *Slfn4* marks a subset of CD11b^{+}Gr-1^{+} MDSCs that coincide with *Helicobacter*-induced gastric metaplasia[6]. Here we demonstrate that SLFN4^{+}-MDSCs modulate their suppressor function by producing MiR130b.

The *MIR130* family has been linked to several types of cancers, including glioma[1820], hepatocellular carcinoma[1121], colorectal[17], pancreatic[22], renal cell[23], endometrial[24], bladder[13], breast[15], as well as gastric cancer[2526]. MIR130b exerts its pro-neoplastic function by modulating multiple signaling pathways and suppressing expression of tumor suppressors such as TP53INP1[11], RUNX3[12], CYLD[1314], or PTEN[15], which promote self-renewal of tumor-initiating cells, proliferation, invasion and migration of various cancer cells. We show here that IFNα-polarized SLFN4^{+}-MDSCs activate the NFκb pathway, which directly induces *MIR130b* expression (Fig.6). Subsequently, MIR130b can sustain persistent activation of NFκb, as previously reported for bladder cancer[13]. Combining our RNA-Seq with in vitro cell line analysis, we surmise that *Cylindromatosis* (*CYLD*) is one of the MIR130b gene targets that likely contributes to SLFN4^{+}-MDSC function. CYLD is a deubiquitinase that can directly interact with an essential modulator of NFκb and the TNFR-associated factor TRAF2 to negatively regulate NFκb activity. It is noteworthy that there are NFκb response elements within the *MIR130b* promoter[13]. Moreover, NFκb modulates multiple signaling pathways, perhaps explaining how MIR130b coordinately regulates several genes.

A by-product of the elevated tissue levels of MIR130b includes detectable levels in the circulation. While other sources of MIR130b likely exist, we observed in both mouse and human blood that elevated MIR130b levels correlate with preneoplastic events in the stomach. Moreover, MIR130b co-localized with human SLFN12L in immune cells surrounding the gastric cancer which coincided with its presence in the blood of these patients. This clinical evidence supports a close association between circulating MIR130b initially with gastric metaplasia that also remains elevated in gastric cancer. Since microRNAs remain stable in the circulation, they can function as biomarkers of disease[8]. Indeed, lymphocytes secrete microvesicles laden with MIR130b that regulate recipient cells[27]. Whether blood levels of circulation MIR130b prove to be a relevant biomarker awaits prospective validation.

Knockdown of MiR130b abolished SLFN4^{+}-MDSC T cell suppressive effect, suggesting that MiR130b was required for acquisition of MDSC function. Specifically, MiR130b suppression abolished *Arg1* and *Nos2* induction, required for MDSC activation. In addition to their immune-suppressive function, MDSCs also affect remodeling of the tumor

microenvironment by producing a variety of cytokines and other molecules that can promote epithelial proliferation[28–30]. Functional microRNAs can be exported and delivered to recipient cells typically by exosomes to regulate target cells. Treating primary myeloid cells, a gastric cell line and gastric organoids with MIR130b mimic showed that MIR130b promotes epithelial cell proliferation. A xenograft model of human-derived gastric cancer organoids further confirmed an essential role of MIR130b in promoting tumor formation. Since MIR130b directly stimulates epithelial cell proliferation, it might also contribute to progression of metaplasia to cancer, in addition to creating a permissive immune microenvironment through T cell suppression.

In summary, we show here that MIR130b has potential as a diagnostic and therapeutic biomarker for gastric metaplasia that progresses to gastric cancer. Indeed, secreted microRNAs are recognized as mediators of intercellular communication and stable circulating biomarkers of disease[8]. Moreover, some clinical trials have now emerged using miRNA-based therapeutics[31].

Materials and Methods:

Transgenic Mice

Gli1$^{nLacZ/nLacZ}$ (referred to *Gli1*$^{-/-}$), *SLFN4-Cre*^{ERT2}*/ Rosa26-tdTomato (SLFN4-tdT)* and *SLFN4-Cre*^{ERT2}*/ Rosa26-tdTomato/Gli1*$^{-/-}$ (*SLFN4-tdT/Gli1*$^{-/-}$) transgenic mouse lines have been previously described[16]. All mice were co-housed under the same specific pathogen-free conditions and were maintained on a genetic background. The University of Michigan and the University of Arizona Institutional Animal Care and Use Committee approved all mouse protocols used in this study.

Patient Samples

Expression of serum MIR130b was determined by qPCR from two cohorts of de-identified human patients: 115 subjects with gastritis from the Institute of Biotechnology in Vietnam (Table S1) (IRBMED; ID: HUM00108090). Detection of *H. pylori* infection was performed using *H. pylori* IgG ELISA and campylobacter-like organism [CLO] test (for active infection). The pathological diagnosis was determined by a GI pathologist blinded to the clinical diagnosis. Eighty-four samples were from Xiangya Hospital (China) (IRBMED; ID: HUM00113773), containing 21 healthy controls and 63 gastric cancer patients (Table S2). Co-localization of MIR130b determined by FISH and SLFN12L determined by immunofluorescence was performed in gastric cancer specimens and normal tissue collected from 5 de-identified patients who underwent surgery at Xiangya Hospital in 2016 (IRBMED; ID: HUM00113773).

Single Cell Preparation for Transcriptome Analysis

Cells isolated from stomach, spleen and bone marrow for RNAseq and microRNA array were prepared as described previously[6]. The single cell suspension from different tissues was flow-sorted to collect Cd11b^{+}SLFN4^{+} and Cd11b^{+}SLFN4^{-} cells based on tdTomato expression, using an iCyt Synergy Flow Sorter (Sony Biotechnology). To obtain sufficient mRNA for analysis, cells isolated and sorted from 5 mice infected with *H. felis* (as described

previously[6]) for 6 months were pooled for one experiment. All 6 groups (ST4+, ST4−, BMS4+, BM4−, SP4+, SPS4−) of cells were from 2 independent experiments. Total RNA was extracted in TRIzol LS Reagent (Invitrogen) and purified using the miRNeasy Mini kit (Qiagen). The RNA integrity was assessed using the Bioanalyzer 2100 system (Agilent Technologies).

Nanostring nCounter miRNA Assay for miRNA Profiling

MiRNA profiling was performed at the UCLA Center for Systems Biomedicine, using the NanoString nCounter® Mouse v1.5 miRNA Expression Assay Kit (NanoString), in which more than 600 pairs of probes specific for a set of miRNAs was combined with a series of internal controls to form the Mouse miRNA Panel Code Set. Details are in the Supplementary Methods.

In Situ Hybridization (ISH) Detection of miRNA

ISH detection of MiR130b was performed using cells cultured on coverslips or paraffin tissue sections. The sections were deparaffinized in xylene and rehydrated in serial ethanol solutions and DEPC-treated water, then digested with 20 μg/ml proteinase K for 5min at 37°C. For both cells and tissues, a prehybridization incubation was performed using a 50% formamide Denhardt's solution for 1h at 55°C. The single strand DNA probes labeled with 5' 6-FAM and 3' DIG were diluted to a working concentration of 50 ng/ml with hybridization buffer and incubated for 24h at 60°C. Samples were washed with 50% formamide in 5x sodium citrate saline (pH 7.0) buffer for 20min at 40°C. Samples were rinsed with DEPC-treated water prior to the diaminobenzidine based immunohistochemistry (Abcam, ab4238) or immunofluorescent staining of SLFN4 or SLFN12L. Probes were purchased from Integrative DNA Technologies, sense probe as a negative control.

MiR130b-3p probe: 5'6-FAM/ATGCCCTTTCATCATTGCACTG/3'DIG

MiR130b-3p control probe: 5'6-FAM/ CAGTGCAATGATGAAAGGGCAT /3'DIG

Cell Culture and Treatment

Thioglycollate (TG)-elicited peritoneal myeloid cells were prepared from the *Slfn4-tdT* mice, as described previously[6]. Cells were treated with 100nM Tamoxifen (Tx, dissolved in DMSO) for 24h to induce Cre recombinase activity and tdTomato expression ex vivo. The Hsa-MIR130b-3p miRNA mimic (50nM, Applied Biological Materials, MCH01270) and the mimic negative control (MCH00000) were transfected into cells using Lipofectamine LTX with PLUS reagent (Thermo Fisher). The Mmu-Mir130b-3p miRNA antisense (CAGUGCAAUGAUGAAAGGGCAU) (10nM, MSTUD0173, Sigma Aldrich), *Slfn4* siRNA or the scrambled controls were transfected using Lipofectamine RNAiMAX transfection reagent (Thermo Fisher) for 48h. To induce *Slfn4* expression, the cells were treated with 800U/ml recombinant IFNα (R&D, #12125-1) for 24h or at different time points.

T Cell Suppression Assay

Carboxyfluorescein Diacetate Succinimidyl Ester based T cell suppression assay was performed as described previously[6]. Peritoneal cells isolated from *Slfn4*-tdT mice were treated with IFNα (800U/ml) for 24h and then flow-sorted for $SLFN4^+$ (tdTomato, red) and $SLFN4^-$ cells (Fig.3B). $SLFN4^+$ and $SLFN4^-$ cells were then transfected with MiR130b mimic, antisense or scrambled control for 48h. Suppression of T cell proliferation was assayed after the addition of $SLFN4^+$ or $SLFN4^-$ cells for 3 days at a T cell/SLFN4 cell ratio of 10:1. Cell proliferation was analyzed using an Attune Acoustic Focusing cytometer (Applied Biosystem).

In Vivo RNAi Transfection

MiR130b antisense or scrambled control were combined with a lipid-based *in vivo* RNAi transfection reagent Invivofectamine 3.0 (Invitrogen) according to the manufacture's instruction. The complexes were then injected intraperitoneally at 1.5mg/kg into three mice infected *H. felis* for 4 months. Three wks after the infection, the mice were necropsied and their stomachs were collected for histological staining and a single cell suspension was generated for flow cytometry.

Organoid/cell Co-culture

Mouse gastric organoids suspended in the Matrigel were seeded in each well, and then overlaid with gastric organoid media as described above. Peritoneal myeloid cells treated with IFNα as described above were flow- sorted into $SLFN4^+$ or $SLFN4^-$ groups. Next 10^5 of either $SLFN4^+$ or $SLFN4^-$ cells were plated onto the 24mm polycarbonate membrane insert (0.4 μm pore diameter; Corning) with 0.5% FBS in growth media. To initiate the co-culture, inserts were combined with the wells for an additional 48h.

Xenograft Assay

Tumor derived organoid lines were generated using the stomach tissue from 3 gastric cancer patients following a previously described protocol[32]. TGO1 was from a diffuse type, TGO2 was from an intestinal type; TGO4 was from a poorly-differentiated adenocarcinoma with diffuse and signet ring cell types. The organoids transfected with MIR130b mimic, antisense or scrambled and cultured for 48h were injected subcutaneously in the right flank of NSG mice. Morphometrics (tumor height, length and width) were measured with a caliper every four days. Tumor volume was calculated using a published equation[33]. The cell viability assay was performed on organoids transfected with Mimic/antisense/scrambled prior to xenograft transplantation (Fig.S6) by flow cytometry using LIVE/DEAD™ Viability/ Cytotoxicity Kit (Thermo Fisher, #L3224).

Real-time Quantitative PCR

Total RNA from cells was extracted in TRIzol (Invitrogen) and purified with the RNeasy Minikit (Qiagen). The qPCR was performed as described previously[6], using the primer sequences described in Table S3.

For detection of *miR130b*, total RNA was extracted from 200μl serum using the miRNeasy Serum/Plasma Kit (Qiagen). Before RNA extraction, *C.elegans* miRNA cel-miR39 miRNA mimic (Cat#219610, Qiagen) was used to spike the serum samples as an endogenous control for normalization during extraction. The stem-loop reverse transcription and subsequent qPCR was performed using the Hsa-MIR130b Real-time RT-PCR detection and cel-miR-39-3p calibration kit (#MBS8244866, Mybiosource) according to the manufacturer's instructions. Stem-loop RT primers specific for *MIR130b* and cel-*mir39*-3p bind to the 3' portion of miRNA for transcription with reverse transcriptase. The RT product was quantified using real-time PCR that includes a specific primer set and SYBR Green dye under the following conditions: initial denaturation at 95°C for 3m followed by 40 cycles of denaturation at 95°C for 12s; annealing and extension at 62°C for 40s. Fluorescence was detected using the CFX96 real-time PCR detection system (Bio-RAD).

Statistics

For qPCR and proliferation experiments, statistical analysis for significance was performed on the log-transformed values using 1-way ANOVA with Tukey's Post-Hoc test for multiple comparisons (GraphPad Prism). All data was expressed as the median with the interquartile range. $P<0.05$ were considered statistically significant. The number of samples per group and replicate experiments are indicated in the figure legends.

Supplementary Material

Refer to Web version on PubMed Central for supplementary material.

Acknowledgements

Support from R01DK118563-01 (to JLM) and P01DK062041-15 (to JLM), the University of Michigan Digestive Disease Center P30DK34933-31, and National Natural Science Foundation of China (No. 81974064). The miRNA profiling using NanoString technology was performed by the UCLA Integrated Molecular Technologies Core/ Center for system Biomedicine supported by the UCLA DDRC_CURE grant P30DK41301-26.

References

1. El-Zaatari M, Kao JY, Tessier A, et al. Gli1 deletion prevents Helicobacter-induced gastric metaplasia and expansion of myeloid cell subsets. PLoS One 2013;8(3):e58935. doi: 10.1371/journal.pone.0058935 [published Online First: 2013/03/23] [PubMed: 23520544]
2. Goldenring JR, Nam KT, Wang TC, et al. Spasmolytic polypeptide-expressing metaplasia and intestinal metaplasia: time for reevaluation of metaplasias and the origins of gastric cancer. Gastroenterology 2010;138(7):2207–10, 10 e1. doi: 10.1053/j.gastro.2010.04.023 [published Online First: 2010/05/11] [PubMed: 20450866]
3. Gabrilovich DI. Myeloid-Derived Suppressor Cells. Cancer Immunol Res 2017;5(1):3–8. doi: 10.1158/2326-6066.CIR-16-0297 [published Online First: 2017/01/06] [PubMed: 28052991]
4. Geserick P, Kaiser F, Klemm U, et al. Modulation of T cell development and activation by novel members of the Schlafen (slfn) gene family harbouring an RNA helicase-like motif. Int Immunol 2004;16(10):1535–48. doi: 10.1093/intimm/dxh155 [published Online First: 2004/09/08] [PubMed: 15351786]
5. van Zuylen WJ, Garceau V, Idris A, et al. Macrophage activation and differentiation signals regulate schlafen-4 gene expression: evidence for Schlafen-4 as a modulator of myelopoiesis. PLoS One 2011;6(1):e15723. doi: 10.1371/journal.pone.0015723 [published Online First: 2011/01/21] [PubMed: 21249125]

6. Ding L, Hayes MM, Photenhauer A, et al. Schlafen 4-expressing myeloid-derived suppressor cells are induced during murine gastric metaplasia. J Clin Invest 2016;126(8):2867–80. doi: 10.1172/JCI82529 [published Online First: 2016/07/19] [PubMed: 27427984]
7. Gabrilovich DI, Ostrand-Rosenberg S, Bronte V. Coordinated regulation of myeloid cells by tumours. Nat Rev Immunol 2012;12(4):253–68. doi: 10.1038/nri3175 [published Online First: 2012/03/23] [PubMed: 22437938]
8. Boon RA, Vickers KC. Intercellular transport of microRNAs. Arterioscler Thromb Vasc Biol 2013;33(2):186–92. doi: 10.1161/ATVBAHA.112.300139 [published Online First: 2013/01/18] [PubMed: 23325475]
9. Mitchell PS, Parkin RK, Kroh EM, et al. Circulating microRNAs as stable blood-based markers for cancer detection. Proc Natl Acad Sci U S A 2008;105(30):10513–8. doi: 10.1073/pnas.0804549105 [published Online First: 2008/07/30] [PubMed: 18663219]
10. Bronte V, Zanovello P. Regulation of immune responses by L-arginine metabolism. Nat Rev Immunol 2005;5(8):641–54. doi: 10.1038/nri1668 [published Online First: 2005/08/02] [PubMed: 16056256]
11. Ma S, Tang KH, Chan YP, et al. miR-130b Promotes CD133(+) liver tumor-initiating cell growth and self-renewal via tumor protein 53-induced nuclear protein 1. Cell Stem Cell 2010;7(6):694–707. doi: 10.1016/j.stem.2010.11.010 [published Online First: 2010/11/30] [PubMed: 21112564]
12. Lai KW, Koh KX, Loh M, et al. MicroRNA-130b regulates the tumour suppressor RUNX3 in gastric cancer. Eur J Cancer 2010;46(8):1456–63. doi: 10.1016/j.ejca.2010.01.036 [published Online First: 2010/02/24] [PubMed: 20176475]
13. Cui X, Kong C, Zhu Y, et al. miR-130b, an onco-miRNA in bladder cancer, is directly regulated by NF-kappaB and sustains NF-kappaB activation by decreasing Cylindromatosis expression. Oncotarget 2016;7(30):48547–61. doi: 10.18632/oncotarget.10423 [published Online First: 2016/07/09] [PubMed: 27391066]
14. Sun B, Li L, Ma W, et al. MiR-130b inhibits proliferation and induces apoptosis of gastric cancer cells via CYLD. Tumour Biol 2016;37(6):7981–7. doi: 10.1007/s13277-015-4632-3 [published Online First: 2015/12/30] [PubMed: 26711782]
15. Miao Y, Zheng W, Li N, et al. MicroRNA-130b targets PTEN to mediate drug resistance and proliferation of breast cancer cells via the PI3K/Akt signaling pathway. Sci Rep 2017;7:41942. doi: 10.1038/srep41942 [published Online First: 2017/02/07] [PubMed: 28165066]
16. Lv M, Zhong Z, Chi H, et al. Genome-Wide Screen of miRNAs and Targeting mRNAs Reveals the Negatively Regulatory Effect of miR-130b-3p on PTEN by PI3K and Integrin beta1 Signaling Pathways in Bladder Carcinoma. Int J Mol Sci 2016;18(1) doi: 10.3390/ijms18010078 [published Online First: 2017/01/04]
17. Colangelo T, Fucci A, Votino C, et al. MicroRNA-130b promotes tumor development and is associated with poor prognosis in colorectal cancer. Neoplasia 2013;15(9):1086–99. [published Online First: 2013/09/13] [PubMed: 24027433]
18. Xiao ZQ, Yin TK, Li YX, et al. miR-130b regulates the proliferation, invasion and apoptosis of glioma cells via targeting of CYLD. Oncol Rep 2017;38(1):167–74. doi: 10.3892/or.2017.5651 [published Online First: 2017/05/24] [PubMed: 28534976]
19. Jia J, Liu Y, Zhang X, et al. Regulation of iNOS expression by NF-kappaB in human lens epithelial cells treated with high levels of glucose. Invest Ophthalmol Vis Sci 2013;54(7):5070–7. doi: 10.1167/iovs.13-11796 [published Online First: 2013/07/03] [PubMed: 23812491]
20. Malzkorn B, Wolter M, Liesenberg F, et al. Identification and functional characterization of microRNAs involved in the malignant progression of gliomas. Brain Pathol 2010;20(3):539–50. doi: 10.1111/j.1750-3639.2009.00328.x [published Online First: 2009/09/25] [PubMed: 19775293]
21. Liu AM, Yao TJ, Wang W, et al. Circulating miR-15b and miR-130b in serum as potential markers for detecting hepatocellular carcinoma: a retrospective cohort study. BMJ Open 2012;2(2):e000825. doi: 10.1136/bmjopen-2012-000825 [published Online First: 2012/03/10]
22. Zhao G, Zhang JG, Shi Y, et al. MiR-130b is a prognostic marker and inhibits cell proliferation and invasion in pancreatic cancer through targeting STAT3. PLoS One 2013;8(9):e73803. doi: 10.1371/journal.pone.0073803 [published Online First: 2013/09/17] [PubMed: 24040078]

23. Wu X, Weng L, Li X, et al. Identification of a 4-microRNA signature for clear cell renal cell carcinoma metastasis and prognosis. PLoS One 2012;7(5):e35661. doi: 10.1371/journal.pone.0035661 [published Online First: 2012/05/25] [PubMed: 22623952]
24. Dong P, Karaayvaz M, Jia N, et al. Mutant p53 gain-of-function induces epithelial-mesenchymal transition through modulation of the miR-130b-ZEB1 axis. Oncogene 2013;32(27):3286–95. doi: 10.1038/onc.2012.334 [published Online First: 2012/08/01] [PubMed: 22847613]
25. Duan J, Zhang H, Qu Y, et al. Onco-miR-130 promotes cell proliferation and migration by targeting TGFbetaR2 in gastric cancer. Oncotarget 2016;7(28):44522–33. doi: 10.18632/oncotarget.9936 [published Online First: 2016/06/16] [PubMed: 27304191]
26. Kim BH, Hong SW, Kim A, et al. Prognostic implications for high expression of oncogenic microRNAs in advanced gastric carcinoma. J Surg Oncol 2013;107(5):505–10. doi: 10.1002/jso.23271 [published Online First: 2012/09/22] [PubMed: 22996433]
27. Pan S, Yang X, Jia Y, et al. Microvesicle-shuttled miR-130b reduces fat deposition in recipient primary cultured porcine adipocytes by inhibiting PPAR-g expression. J Cell Physiol 2014;229(5):631–9. doi: 10.1002/jcp.24486 [published Online First: 2013/12/07] [PubMed: 24311275]
28. Casella I, Feccia T, Chelucci C, et al. Autocrine-paracrine VEGF loops potentiate the maturation of megakaryocytic precursors through Flt1 receptor. Blood 2003;101(4):1316–23. doi: 10.1182/blood-2002-07-2184 [published Online First: 2002/10/31] [PubMed: 12406876]
29. Shojaei F, Wu X, Qu X, et al. G-CSF-initiated myeloid cell mobilization and angiogenesis mediate tumor refractoriness to anti-VEGF therapy in mouse models. Proc Natl Acad Sci U S A 2009;106(16):6742–7. doi: 10.1073/pnas.0902280106 [published Online First: 2009/04/07] [PubMed: 19346489]
30. Lindau D, Gielen P, Kroesen M, et al. The immunosuppressive tumour network: myeloid-derived suppressor cells, regulatory T cells and natural killer T cells. Immunology 2013;138(2):105–15. doi: 10.1111/imm.12036 [published Online First: 2012/12/12] [PubMed: 23216602]
31. Chakraborty C, Sharma AR, Sharma G, et al. Therapeutic miRNA and siRNA: Moving from Bench to Clinic as Next Generation Medicine. Mol Ther Nucleic Acids 2017;8:132–43. doi: 10.1016/j.omtn.2017.06.005 [published Online First: 2017/09/18] [PubMed: 28918016]
32. Bertaux-Skeirik N, Centeno J, Gao J, et al. Oncogenic Transformation of Human-Derived Gastric Organoids. Methods Mol Biol 2016 doi: 10.1007/7651_2016_4 [published Online First: 2016/08/20]
33. Tomayko MM, Reynolds CP. Determination of subcutaneous tumor size in athymic (nude) mice. Cancer Chemother Pharmacol 1989;24(3):148–54. [published Online First: 1989/01/01] [PubMed: 2544306]

Summary Box

1. What is already known: The myeloid differentiation factor Schlafen4 (Slfn4) marks a subset of Myeloid Derived Suppressor Cells (MDSCs) in the stomach during *Helicobacter*-induced SPEM, which is an early committed step appearing prior to gastric cancer.
2. What are the new findings? MIR130b produced by SLFN4+ MDSCs plays an essential role in MDSC function and in the metaplastic changes prior to gastric cancer.
3. How might it impact clinical practice? MIR130b has potential as an early non-invasive diagnostic and therapeutic biomarker for gastric metaplasia that could progress to gastric cancer.

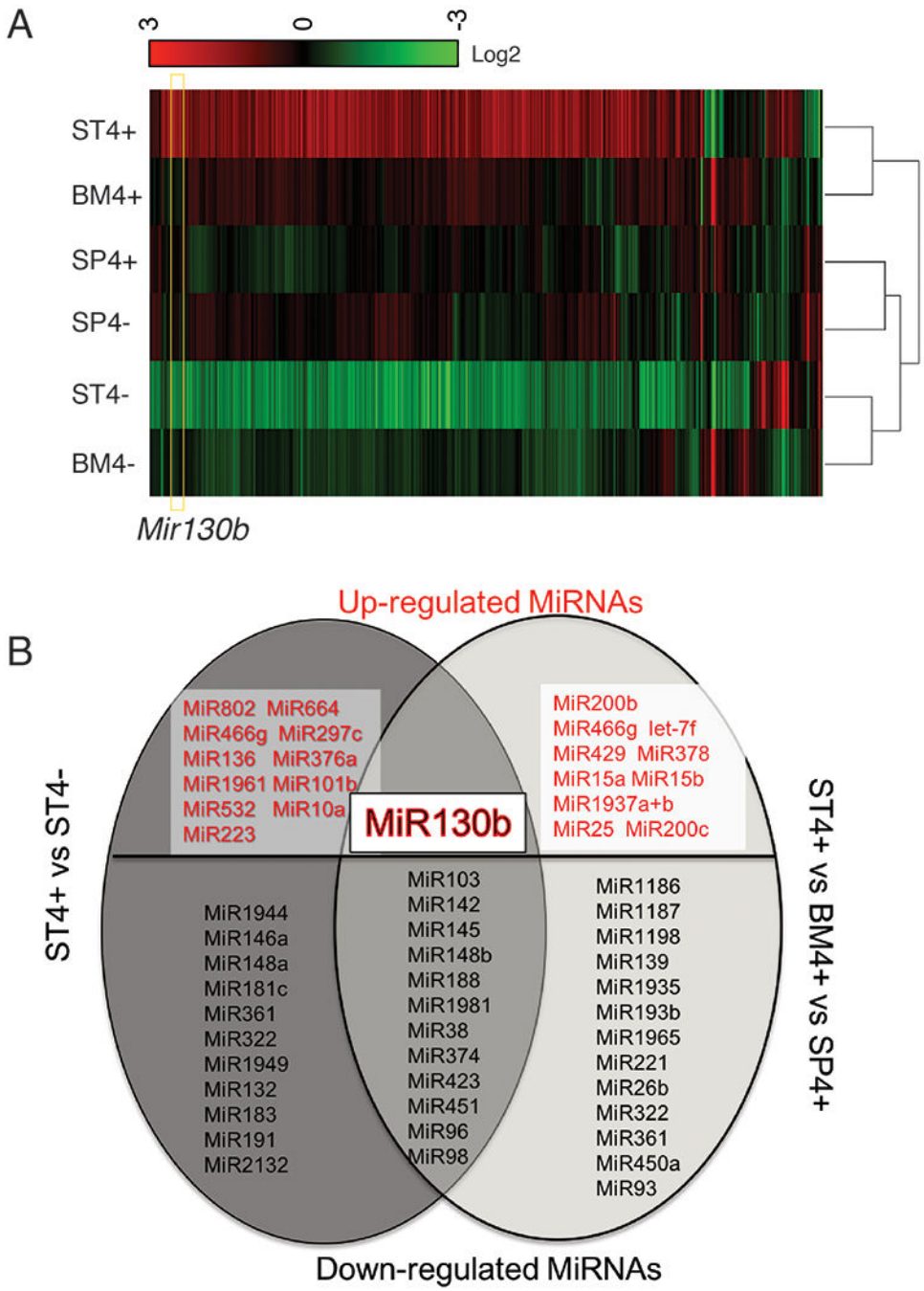

Figure 1. MiRNA analysis of SLFN4^{+} cells with miRNA profiling.

WT chimeric mice reconstituted with *Slfn4*-tdT bone marrow were treated with Tx two weeks prior to euthanization. SLFN4^{+} vs SLFN4^{-} cells sorted from stomach (ST4+/−), spleen (SP4+/−) and bone marrow (BM4+/−) were profiled by the miRNA NanoString nCounter Array. A) Cluster analysis of differentially-expressed miRNAs B) A Venn diagram of the up- and down-regulated miRNAs in ST4+ vs ST4- and ST4+vs SP4+vs BM4+ after miRNA profiling. Each sample was pooled from 5 mice. N=2 separate flow sorts. One-way ANOVA test. Cutoff value: P <0.05.

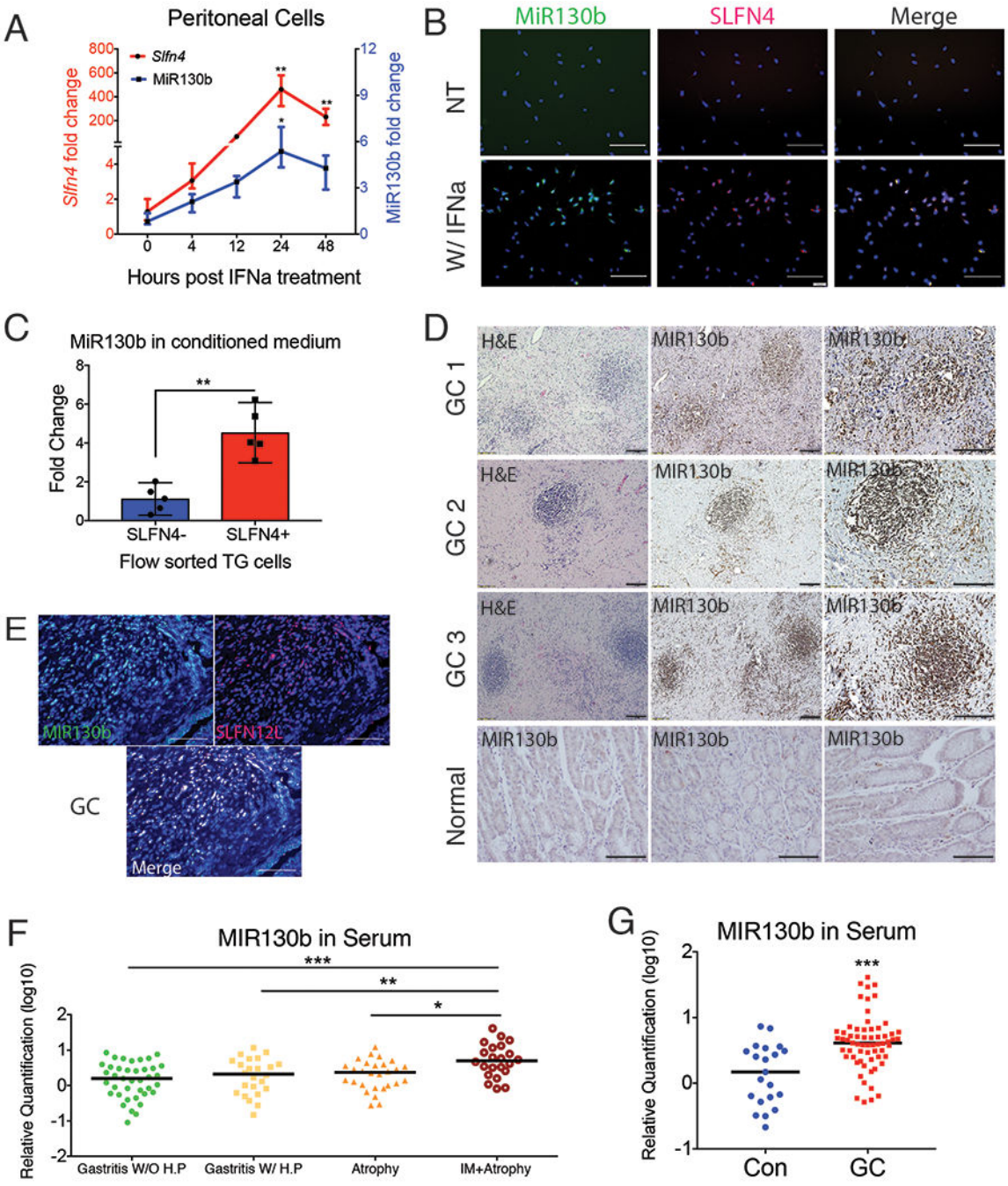

Figure 2. MIR130b correlates with mouse SLFN4 and human SLFN12L expression.

Thioglycollate-elicited peritoneal cells collected from *Slfn4*-tdT mice were treated with IFNα (800U/ml) or were non-treated (NT). A) Time course of mRNA expression for *Slfn4* and MiR130b were analyzed by qPCR and B) by FISH for MiR130b (green) co-localizing with immunofluorescent staining for *Slfn4*-tdT (red). N=5 expts. Scale bar=50μm. One-way ANOVA followed by Tukey's multiple comparisons test on log-transformed values. P-values are relative to UI or time 0. C) Flow-sorted SLFN4+ vs SLFN4− cells after IFNα treatment were cultured for 24 hours for collecting conditioned media. MiR130b secreted into the

media were determined by qPCR. Mann-Whitney U test was performed. D) Combined MIR130b ISH and IHC detection in normal tissue and gastric cancer tissue collected from gastric cancer patients. Representative staining from 5 patients. Same tissues were detected by E) FISH with MIR130b (green) followed by immunofluorescent staining for SLFN12L (red). Scale bar=100μm. Serum MIR130b levels were determined by qPCR in F) Gastritis patients, N=27-31 per group for 4 groups of patients: Gastritis without active *H. pylori* infection (IgG+,CLO−); Gastritis with active *H. pylori* infection (CLO+); with atrophy and with intestinal metaplasia. P-values are relative to gastritis without active *H. pylori* infection group. and in G) Gastric cancer patients, N=21-63 per group. Significance was determined using Kruskal-Wallis ANOVA with Dunn's test of multiple comparisons. *P<0.05, **P<0.01, ***P<0.001. Horizontal lines represent the median and interquartile range.

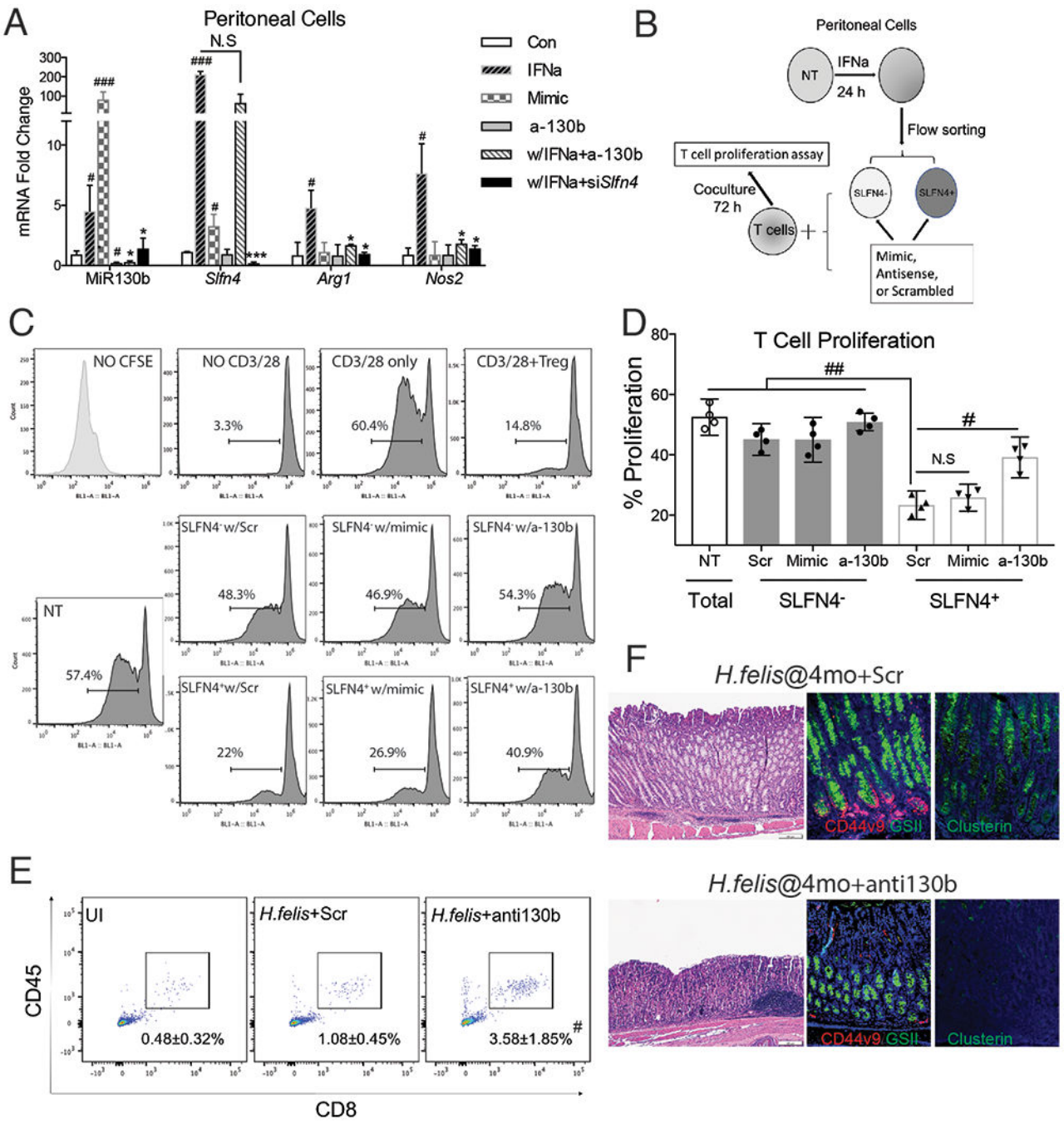

Figure 3. MiR130b is essential for SLFN4^{+}-MDSC activity.

A) Thioglycollate (TG)-elicited peritoneal myeloid cells (PCs) collected from WT mice were transfected with MiR130b mimic, antisense MiR130b, *Slfn4* siRNA or scrambled control (Scr), and then treated with IFNα (800U/ml) or PBS for 24h. Differential gene expression was evaluated by qPCR. N=5 expts. B) Protocol to collect SLFN4^{+} cells for co-culture with T cells. TG-elicited PCs from *Slfn4*-tdT mice were treated with IFNα for 24h and then flow-sorted for SLFN4 $^{+}$ and SLFN4 $^{-}$ cells. Sorted cells were then transfected with MiR130b mimic, antisense or Scr. These sorted cells and non-treated peritoneal cells

(NT) were co-cultured with activated T cells for 72h. C) CFSE-based T cell suppression assay was quantified by flow cytometry. The top 4 representative histograms show proliferation of control groups: NO CFSE, without anti-CD3/28 microbeads activation, with CD3/28 but without cell co-culture, and co-cultured with Tregs ($CD4^+CD25^+$). The median percentage of proliferating T cells is shown in the representative histograms and plotted for N=4 expts in the D) scatter graph. NT, non-treated. One-way ANOVA followed by Tukey's multiple comparisons test on log-transformed values. The mice infected with *H.felis* for 4 months were treated with antisense MIR130b or scrambled control using Invivofectamine. Three wks post injection, E) $CD45^+CD8^+$ cytotoxic T cells in the stomach were detected by flow cytometry and F) Metaplastic change was shown by H&E, CD44 variant 9 (red), GSII (green) and clusterin (green) staining. UI, uninfected. N=3 expts. *P-values are relative to IFNα-treated group. #P-values are relative to CON or scrambled. *or #P<0.05, **or ##P<0.01, ***or ###p<0.001, ####P<0.0001. NS, not significant. The median and interquartile range is shown.

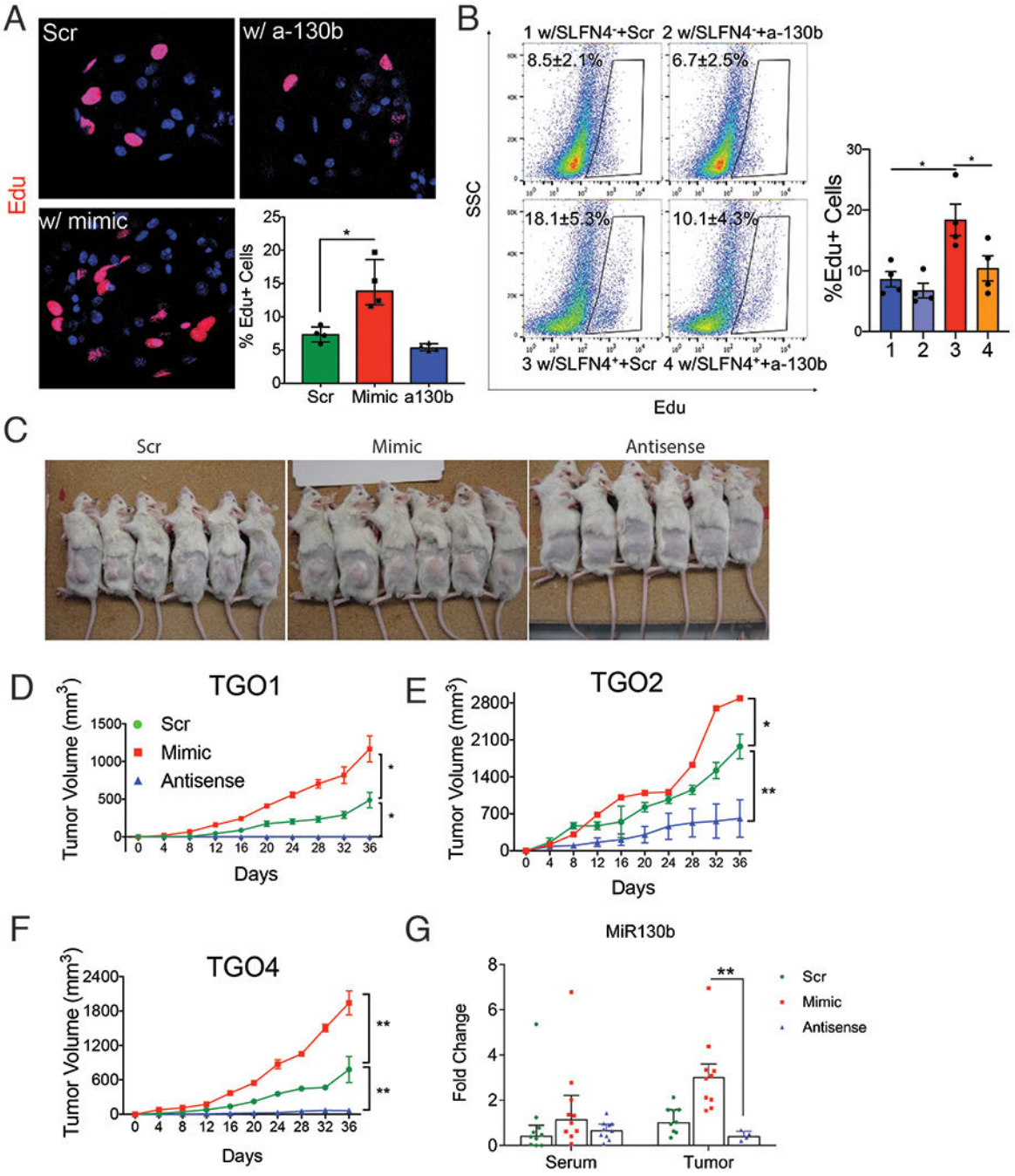

Figure 4. MiR130b promotes gastric epithelial cell proliferation and xenograft tumor formation.

Gastric organoids from wildtype mice were A) transfected with MiR130b mimic, antisense MiR130b or scrambled control (Scr) or B) co-cultured with flow-sorted SLFN4− or SLFN4+ cells transfected with MiR130b antisense or Scr in the trans-well system for 48 hours. Organoids were then stained with EdU antibody. EdU+ cell were visualized by A) confocal or B) quantified by flow cytometry. N=4 expts. Xenograft assays were performed by injecting 3 human gastric cancer patient derived organoid lines (TGO1 = Diffuse type; TGO2=intestinal type; TGO4= poorly differentiated with signet ring cells) transfected with

MiR130b mimic, antisense or Scr subcutaneously in the right flank of NSG mice. C) Mice at the end point of the xenograft assay. Tumor height (h), length (l) and width (w) from 3 different xenograft D-F) were measured every 4 days using a caliper. Tumor volume was plotted over a 36-day time course post-transplant. * significance compared to Scr group. G) MiR130b expression determined by RT-qPCR in NSG mouse serum and tumor tissue. TGO, tumor gastric organoid. One-way ANOVA followed by Tukey's multiple comparisons test on log-transformed values. N=10 mice in 3 expts. *P<0.05, **P<0.01. Horizontal lines represent the median and interquartile range.

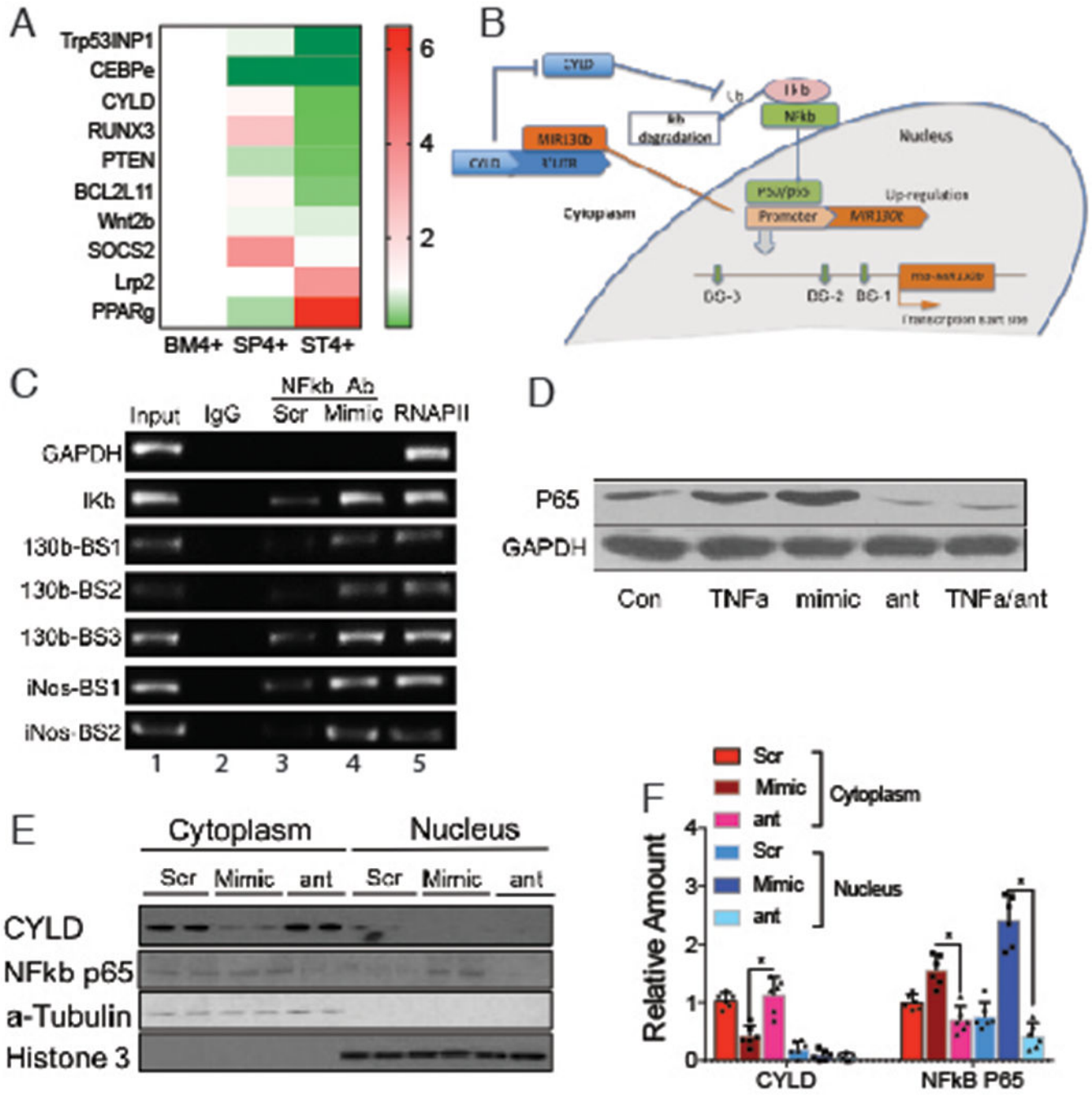

Figure 5. MIR130b targets Cylindromatosis (*CYLD*) and induces NFkb activity.

A) Microarray heat map of MIR130b candidate targets predicted by TargetScan or reported previously. Samples were pooled from 5 mice per expt. N=2 expts. B) Hypothetical model illustrating the NFκB/*MIR130b*/CYLD axis and schematic of a typical *MIR130b* promoter. The predicted NFκB binding sites were located at −229 to −239, −474 to −484, and −1467 to −1477 upstream of the transcription start site. NFκB upregulates the transcription of *MIR130b*, which target and decreases CYLD expression and disrupts the negative feedback of CYLD on NFκB activation. This axis keeps the constitutive activation of NFκB. C)

Chromatin immunoprecipitation (ChIP) assay using HL-60 cells showed that activity of NFκB physically bound with the promoters[13] as indicated (Supplementary Methods). Lane 1, input chromatin prior to immunoprecipitation. Lane 2, immunoprecipitation with a non-specific antibody (IgG). Lane 3-4, immunoprecipitation with NFκB P65 antibody after the cells were transfected with lane 3 scrambled control (Scr) or lane 4 MIR130b mimic. Lane 5, immunoprecipitation with RNA polymerase II (RNAP II) antibody as a positive control. D) HL-60 cells were treated with TNFα, MIR130b mimic, antisense (ant), or TNFα plus MIR130b antisense (TNFα/ant). NFkb p65 expression was determined by Western blotting. GAPDH as a loading control. N=5 expts. CYLD and NFkB-p65 expression in cytoplasm and nucleus of xenograft tumors of scrambled control (Scr), mimic and anti-130b (ant) groups were E) determined by Western blot analysis and was F) quantified using ImageJ. α-tubulin and histone-3 served as cytoplasmic and nucleic loading control, respectively. N=3 expts. One-way ANOVA followed by Tukey's multiple comparisons test on log-transformed values. *P<0.05, The median ± interquartile range.

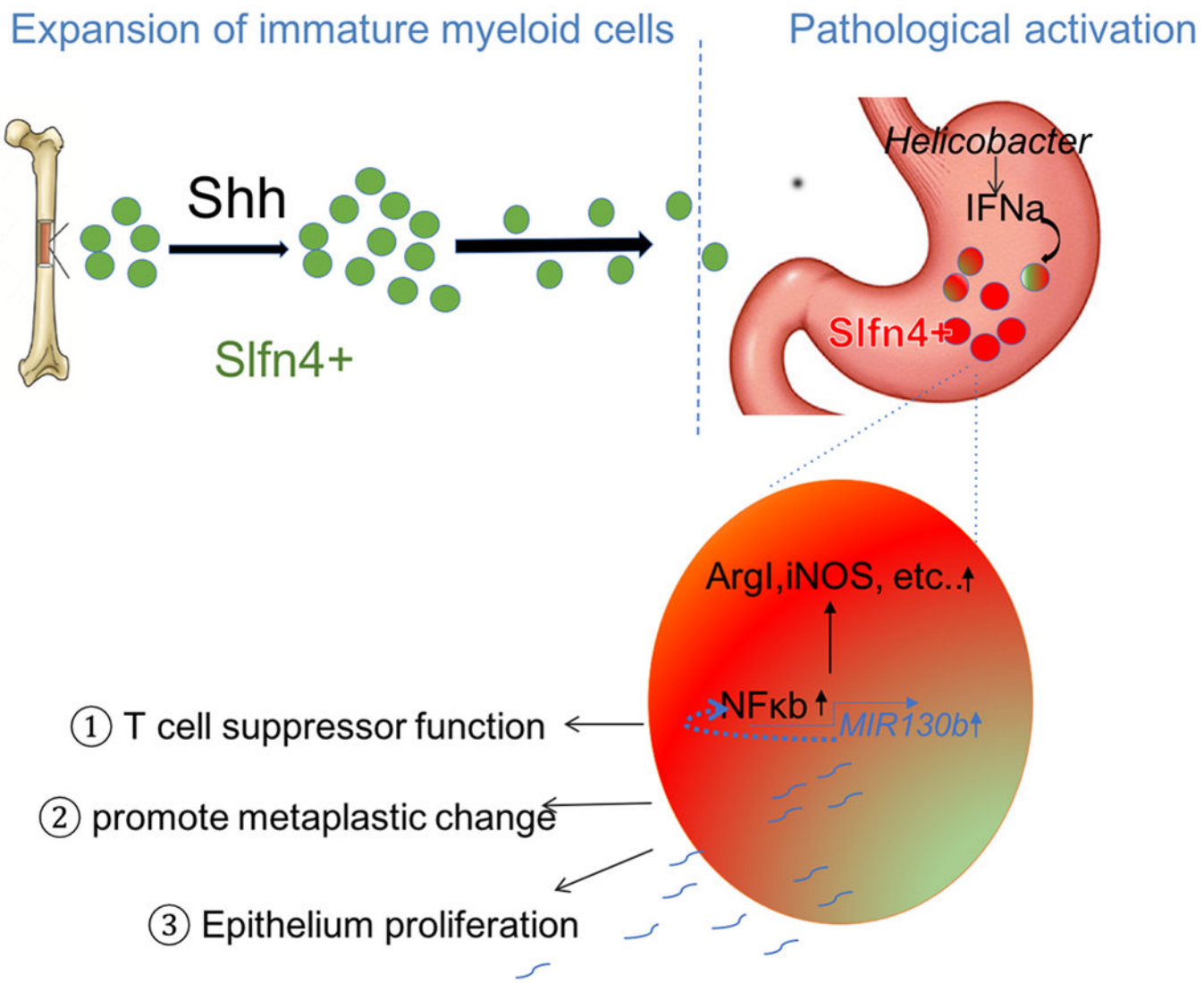

Figure 6. Schematic of SLFN4+-MDSCs polarized in the stomach during *Helicobacter* infection.

Acute Sonic hedgehog (SHH) release by parietal cells into the circulation is sensed by BM-derived SLFN4^{+} myeloid cells (green), which home to the infected stomach. Eventually, the SLFN4^{+} myeloid cells become activated and polarized to MDSCs (red) and accumulate in response to tissue IFNα produced during chronic *Helicobacter* infection. There is a feedback loop between NFκb activation and MIR130b expression in SLFN^{+}-MDSCs (enlarged red cell). MiR130b produced by SLFN^{+}-MDSCs 1) regulate T cell suppressor function, 2) affect epithelial cell proliferation; 3) promote metaplastic changes.